Prasert Prapamonthon
Key Laboratory for Mechanics in Fluid Solid Coupling Systems,
Institute of Mechanics,
Chinese Academy of Sciences,
Beijing 100190, China;
Department of Aeronautical Engineering,
International Academy of Aviation Industry,
King Mongkut's Institute of Technology Ladkrabang,
Bangkok 10520, Thailand
e-mails: jinfa@imech.ac.cn;
prasert.pr@kmitl.ac.th

Bo Yin[1]
Key Laboratory for Mechanics in Fluid Solid Coupling Systems,
Institute of Mechanics,
Chinese Academy of Sciences,
Beijing 100190, China
e-mail: yinbo@imech.ac.cn

Guowei Yang
Key Laboratory for Mechanics in Fluid Solid Coupling Systems,
Institute of Mechanics,
Chinese Academy of Sciences,
Beijing 100190, China
e-mail: gwyang@imech.ac.cn

Mohan Zhang
School of Engineering Science,
University of Chinese Academy of Sciences,
Beijing 100049, China
e-mail: zhangmohan@imech.ac.cn

Separate and Combined Effects of Surface Roughness and Thermal Barrier Coating on Vane Cooling Performance

This work investigates separate and combined effects of the vane surface roughness and thermal barrier coating (TBC) on the cooling performance of a film-cooled high-pressure turbine vane using computational fluid dynamics (CFD) with conjugate heat transfer (CHT) analysis. The cooling effectiveness and heat transfer coefficient, where are predicted within an investigated range of the roughness height from 5 to 20 μm, are compared with those of the smooth vane. Results show that the roughness height increases local heat transfer coefficients in general in the suction side (SS) and the rear-half portion of the pressure side (PS), thereby reducing the cooling effectiveness. The results are different from those in the suction-side vicinity of the leading edge (LE) to further downstream of the pressure side due to uncertain local heat transfer coefficients. In addition, thermal sensitivity to the roughness height and TBC is investigated based on the volume basis in the roughness height range which is extended to 120 μm. Results show that without TBC, a 120 μm increase in the roughness height causes 24 K and 20 K rises of the average and maximum vane temperatures, respectively. With TBC, the average and maximum vane temperatures are reduced as much as 18 K and 27.8 K, respectively. [DOI: 10.1115/1.4046428]

Keywords: gas-turbine heat transfer, surface roughness, cooling performance, thermal barrier coating

Introduction

Turbomachines like turbine and compressor are complex mechanical machines that are related to many aspects of mechanical engineering such as aerodynamics, thermodynamics, and heat transfer. With unavoidable operating conditions of gas turbines, turbine airfoils need to operate under high thermal load to obtain high power output and thermal efficiency. As a result, the durability of the turbine airfoils is aggravated, thereby leading to serious damage to the turbine airfoils. Basically, an airfoil of state-of-the-art gas turbines has a highly sophisticated cooling system that consists of internal cooling and external cooling (film cooling) as well as effective thermal barrier coating (TBC) for thermal alleviation. The comprehensive assessment of airfoil surface and structural temperatures, and heat transfer is fundamentally needed because it is beneficial to the accurate prediction of the lifespan of the turbine airfoils under thermal failure. Based on Newton's law of cooling, it is clear that heat convection on turbine airfoils depends on their surface area quantitatively and qualitatively. Previous studies show that surface roughness is a physically important factor that affects aerodynamics, heat transfer, and flow transition on turbine airfoils [1–3]. It is found that the airfoil surface quality is declined by the repeatedly applied thermal load. As a result, the aerothermal performance of the airfoils decreases due to the natural process decline such as the deposition of chemical reaction products and the erosion of TBC. Then, these typical problems lead to the difference of roughness characteristics obtained by manufacturing design and the end of their life eventually. In fact, these problems cause non-uniform roughness distributions on the airfoil surfaces, as previous investigations [4,5]. Hence, understanding of both aerodynamic and thermal behaviors associated with the surface roughness on the turbine airfoils as well as the considerable ability to accurately predict effects of the surface roughness is indispensable, especially on heat transfer surface. Experimental and numerical approaches have been employed to investigate the influence of surface roughness on heat transfer, secondary flow, friction loss, turbulent kinetic energy, and film cooling through flat plates and airfoil models. Based on the experimental approach, Stripf et al. [6] measured external heat transfer on a high-pressure turbine vane with varying surface roughness. Their conclusion indicated a strong influence of roughness on the onset of transition. The results were also drawn that heat transfer coefficients caused by roughness in the turbulent boundary layer increase by up to 50% when compared with the smooth reference surface. Matsuda et al. [7] experimented to investigate the effects of surface roughness of both nozzle and end-wall on a turbine nozzle performance using a liner cascade under Reynolds numbers of $0.3–1.0 \times 10^6$. In their work, many models of surface roughness were used and the increment of nozzle profile loss with Reynolds number for larger roughness group was documented. They also compared the effects of nozzle surface roughness and end-wall roughness and indicated that the increase of the end-wall roughness has a higher effect on the increase of net secondary flow loss. Neuhaus et al. [8] experimented to study the influence of surface roughness on turbulent properties in the wake of a turbine blade. Their results showed that friction loss increases with the extension of roughness.

[1]Corresponding author.

Manuscript received July 15, 2019; final manuscript received February 7, 2020; published online February 22, 2020. Assoc. Editor: W.J. Marner.

Another observation was that roughness results in the extension of the high turbulent kinetic energy regions. Rutledge et al. [9] experimentally studied the effects of roughness on film cooling effectiveness of a turbine vane suction side (SS). They found that at low blowing ratios, roughness reduces film effectiveness because thicker boundary layers caused by rough surfaces can lead to jet lift-off. Furthermore, roughness has a significant influence on local turbulence near the surfaces. This dissipates coolant more rapidly. At high blowing ratios, roughness improves film effectiveness because jet lift-off from the surface is limited. Besides, Demling and Bogard [10] discussed the role of flow path obstructions on film effectiveness and depositing layers of combustion products or eroding TBC on the SS of a gas-turbine vane. According to the numerical approach, it has been developed to accurately predict the effect of roughness on gas-turbine aerodynamics and heat transfer. Models need to have the capability to explain surface roughness effects on boundary layer development and its transition. Most models developed for heat transfer coefficient or skin friction are done based on the equivalent sand-grain roughness in pipes proposed by Nikuradse [11]. This proposal seems different from real situations existing to surfaces roughness of gas-turbine components, but it is still beneficial to the assessment of real roughness on turbine blades for film cooling design as reported by Glasenapp et al. [12]. Some examples of the numerical investigation on surface roughness are mentioned. Boyle et al. [13] identified a numerically appropriate means of predicting the effects of surface roughness on heat transfer on turbine airfoils. They also indicated the strong influence of the role of equivalent roughness height on turbulence models for rough surface heat transfer predictions. Lutum et al. [14] pointed out the role of computational investigation of surface roughness effect on heat transfer on the stator end-wall of an axial turbine. The study of roughness sensitivity using CFD with several transition models has been proposed by open literature [15–17]. More details of a comprehensive review of surface roughness effects in gas turbines are presented by Bons [18].

As previously mentioned, TBC also plays a significant role in the thermal protection in modern gas turbines. The ability and effects of TBC have been reported by several works of literature. Boyle et al. [19] numerically investigated the role of TBC for a high-pressure turbine vane coated with a low conductivity layer thickness of 0.25 mm. Their conclusion was drawn by comparing the stress distribution of the vane with trailing edge (TE) ejection to that without trailing edge ejection. Feist et al. [20] experimentally studied to provide temperature data of a turbine engine with modified TBCs in the hot section at high temperatures. Sadowski and Golewski [21] used CFD and computational structure mechanics to analyze heat transfer and thermal stresses of a coated turbine vane at high temperatures up to 1600 K. Alizadeh et al. [22] used CFD with conjugate heat transfer (CHT) to indicate thermal sensitivity of a turbine blade with different values of TBC thickness and conductivity. They concluded that the addition of TBC results in reducing the overall heat flux of the hot gas to the coolant, thereby reducing temperature gradient within the blade metal. With the variation of the thermal conductivity, they found that when TBC thermal conductivity is low, it greatly turns down the blade temperature. But, when TBC thermal conductivity reached the blade thermal conductivity, it has an insignificant effect on the blade temperature because of the same thermal properties between TBC and blade materials. Prapamonthon et al. [23] studied the effects of TBC on cooling performances of a nozzle guide vane at different turbulence intensities. Some of their conclusion indicated that for all turbulence intensities, TBC plays the positive and negative roles in heat flux at the same time and significantly increases the overall cooling effectiveness in regions which are cooled ineffectively by cooling air emitted from film holes.

Although there have been many numerical and experimental studies of the effects of surface roughness and TBC on aerodynamics and heat transfer of turbine airfoils for many years, a deeper and more comprehensive understanding of the role of physical roughness and TBC is still required because overall thermal problems obtained from a turbine airfoil are complicated by combined modes of heat transfer from hot-wall and cold-wall sides. As reviewed above, flat plates or non-film-cooled vanes or vanes with a small number of film holes were used as the study model. The objective of the present work is to numerically study the cooling performance of a high-pressure turbine vane under real situations caused by separate and combined effects of roughness and TBC, which are of practical use. The turbine vane is cooled by a large number of film holes and impingement holes, i.e., 217 film holes and 347 impingement holes in total. The integration of computational fluid dynamics (CFD) and CHT approaches is applied for this investigation. The present work can provide gas-turbine designers, investigators, and manufacturers with valuable information obtained by numerical prediction of cooling effectiveness, heat transfer coefficient, and aerothermal sensitivity under variation in physical roughness height on the vane surface coated with TBC.

Vane Model, Coolant Passages, and Film Holes

The turbine vane used in this work is one of 46 vanes from the first-stage high-pressure gas turbine, which is adopted from NASA Energy Efficient Engine program by Halila et al. [24]. The vane operates under the mainstream flowing through a passage designed as an annular cascade with an arc sector of 7.826 deg, as shown in Fig. 1(*a*). The configuration of the vane and its cooling passages is shown in Fig. 1(*b*). The vane span is about 4 cm. The external vane surface is cooled by cooling air emitted from 217 film holes of 13 rows, which are connected with two passages of internal cooling passages. All of the film holes are placed orderly, i.e., (1) two rows of fan-shaped holes (R1 and R2) and two rows of cylindrical holes in the radial direction (R3 and R4) on the SS, (2) two rows of cylindrical holes in the radial direction (R5 and R6) on the leading edge (LE), (3) three rows of cylindrical holes in

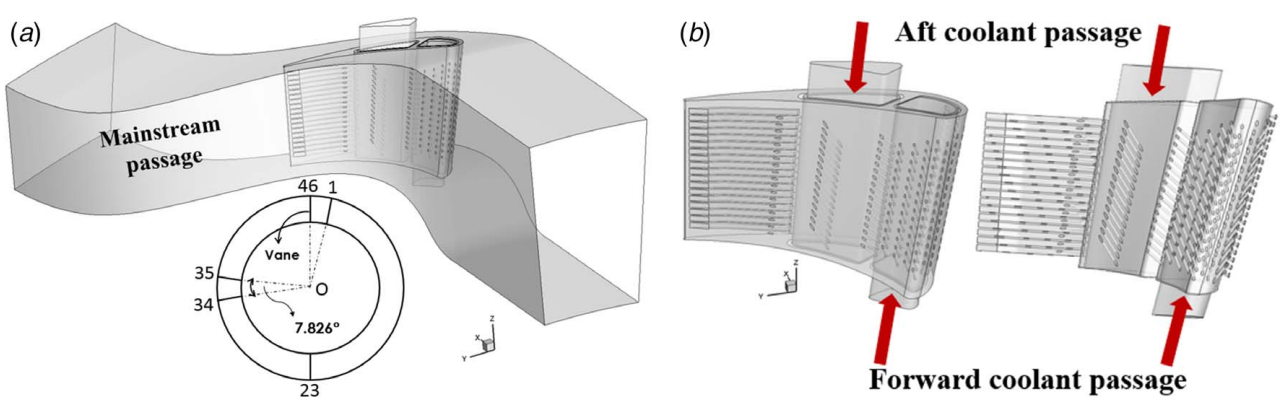

Fig. 1 Configuration of (*a*) mainstream annular cascade and (*b*) vane and its cooling passages

the radial direction (R7, R8, and R9), two rows of cylindrical holes in the compound direction (R10 and R11) and one row of cylindrical holes in the axial direction (R12) on the pressure side (PS), and (4) one row of slots (R13) near the TE, as illustrated in Fig. 2(*a*). The angle of the radial film holes R3–R9 is 25 deg, while the compound angle of the film holes from R10 and R11 is 45 and 60 deg, respectively. More details of the film holes are given in Table 1.

As mentioned previously, the two internal passages of the vane are used for internal cooling and cooling air supply. One is the forward cavity for the film holes located in the SS, the LE, and some part of the PS. The other is the aft cavity for the film holes placed in the TE and the further downstream and rear portion of the PS. To enhance heat convection within the internal cooling passages, a baffle with impingement holes is installed inside the cavities, i.e., 131 and 216 holes for the forward and aft baffles, respectively, as seen in Fig. 2(*b*). The geometric position between the internal vane surface and baffle is arranged with a distance (d) of about 0.45 mm and the impingement holes are arranged in staggered and in-line patterns for the forward and aft baffles, respectively. The impingement holes on both baffles have the same diameter of 0.071 cm and the spacing between the impingement holes varies between six and eight diameters on the aft baffle and four and eight diameters on the forward baffle.

Table 1 Details of film holes used in the present work [24]

Row	Region	Number of holes	Hole diameter, mm	Hole type
1	**SS**	21	**0.610**	Axial, shaped
2	**SS**	22	**0.610**	Axial, shaped
3	**SS**	16	0.508	**Radial**
4	**SS**	16	0.508	**Radial**
5	LE	15	0.508	**Radial**
6	LE	16	0.508	**Radial**
7	**PS**	15	0.508	**Radial**
8	**PS**	14	0.508	**Radial**
9	**PS**	13	0.508	**Radial**
10	**PS**	17	**0.610**	Compound angle, 45 deg
11	**PS**	16	0.508	Compound angle, 60 deg
12	**PS**	18	0.508	**Axial**
13	TE/PS	18	**0.559 × 1.63**	Pressure side slot

Computational Technique and Setup

The computational domain is divided into two parts, i.e., fluid and solid domains. The computational mesh is generated by ANSYS ICEM. H-type meshes are mainly used in the fluid domain and the O-grid method is used to generate meshes with 8–12 layers stretched in the normal direction to the solid walls in order to suffice for resolution of flow in the boundary layer. As mentioned previously, the first stage of this gas turbine consists of 46 nozzle guide vanes, so only one is used for prediction under the periodic boundary condition of the mainstream cascade with the arc sector of 7.826 deg. This can relieve the limitation of time-consuming difficulty and computational cost, but numerical results are still meaningful. Three numbers of mesh elements, i.e., 7, 11, and 16 million elements are considered for mesh independence study. The geometry and computational mesh used in the present study are generated in the same way that Zhang et al. [25] did so that the mesh independence approved by Zhang et al. [25] can be used. The three numbers of the computational mesh were compared in terms of the surface temperature distribution at midspan, as seen in Fig. 3. It was found that the surface

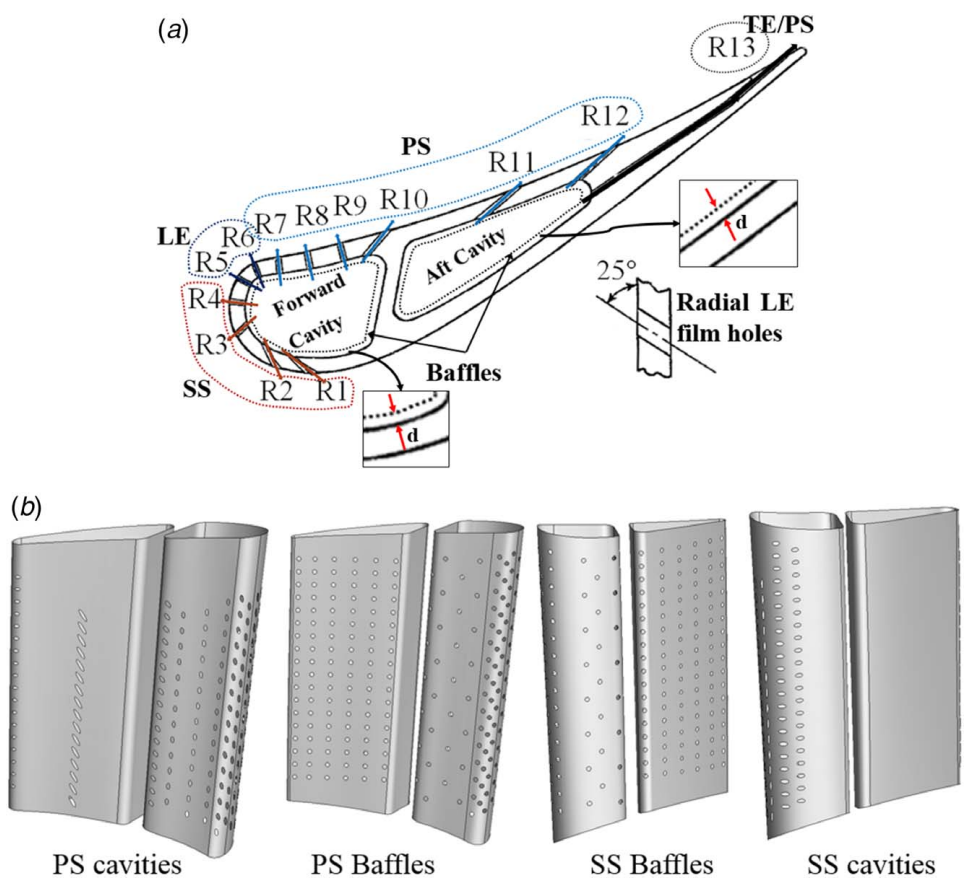

Fig. 2 (*a*) Configuration of film holes at midspan and (*b*) baffles used in the cavities and its impingement holes

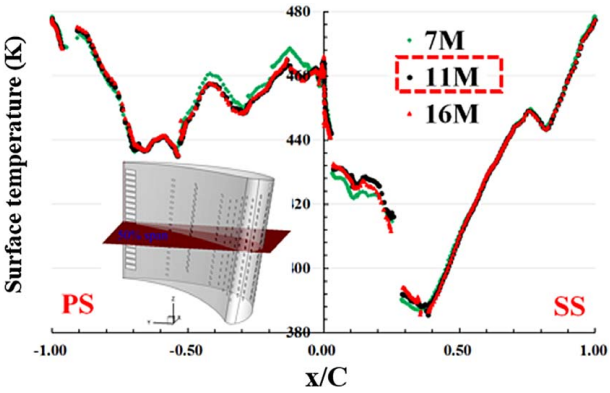

Fig. 3 Mesh independence study done by Zhang et al. [25].

temperature distributions obtained by 11 and 16 million elements agreed well to each other with the maximum error of about 3%. Therefore, it is reasonable to adopt the mesh number of 11 million elements as the computational mesh for the present work. According to this mesh, it has the averaged Y^+ of about 5, which is acceptable for accurate simulation of flow in the boundary layer. Some parts of the computational mesh are depicted in Fig. 4.

The solver for the simulation is ANSYS FLUENT and the shear stress transport (SST) k–ω turbulence model is employed because the present work involves transitional flow. Additionally, so far it has been confirmed by several works of literature [22,26,27] that this turbulence model gives acceptable results that agreed well with experimental data. To decide the solution convergence, the criteria of the convergence are defined by the variation of the continuity and energy residuals, which must be lower than 10^{-3} and 10^{-7}, respectively. The mass flow balance of all inlets and outlets is also checked to ensure that the solutions are in accordance with the conservation of mass. In addition, the six-point surface temperatures on the PS, LE, SS, and TE are monitored to confirm the convergence of the numerical results. Exactly, the six-point temperatures must keep unchanged with the subsequent iterations. Because the present work addresses the heat transfer problem by means of CHT, mesh interface technique

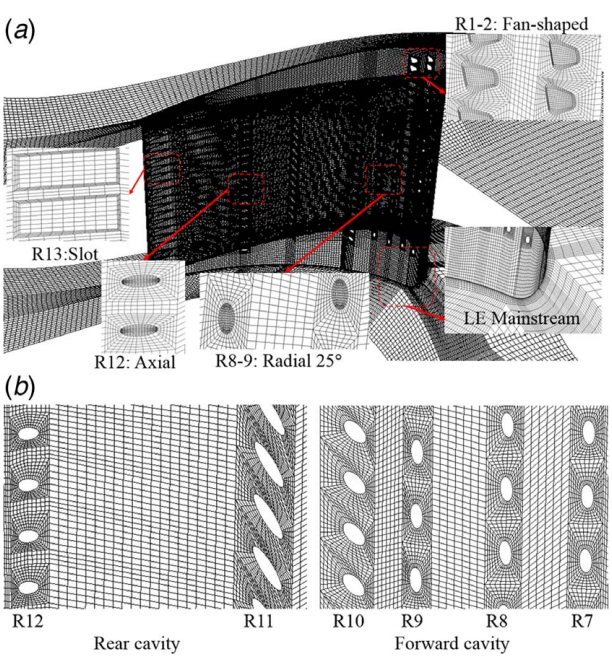

Fig. 4 Computational mesh of solid and fluid domains: (*a*) solid, fluid, and film holes and (*b*) cavities

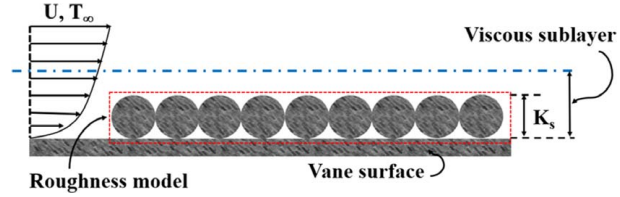

Fig. 5 Uniform roughness model for vane surfaces

is applied at surfaces between the solid and fluid domains for heat flux transfer. With this technique, the temperature at solid/fluid interfaces is equivalent to each other. For TBC effects, the vane is coated with a uniform TBC layer with a thickness of 355.6 μm. This thickness is the same value used in the report [24]. Following the very thin thickness of the TBC, heat transfer within the TBC layer is considered as 1D heat conduction using the thin-wall model available in ANSYS FLUENT. To predict the roughness effects on the cooling performance, the vane surface roughness, which refers to any regularities on the vane surface, is modeled as a uniform sand-grain roughness, as illustrated in Fig. 5. According to this model, two parameters are used, i.e., roughness constant (C_s) and physical roughness height (K_s). It should be noted that as previously studied by Nikuradse [11], the physical roughness height is related to the nondimensional roughness height (K_s^+) as Eq. (1)

$$K_s^+ = \frac{K_s u^*}{\nu} \tag{1}$$

where $u^* = C_\mu^{0.25} k^{0.5}$ and ν represents the kinematic viscosity. C_μ is a constant of 0.09 and k is the turbulence kinetic energy. Furthermore, the physical roughness depends upon the K_s^+ value. Characteristically, three roughness regimes are separately defined by K_s^+, namely, (a) hydrodynamically smooth surface ($K_s^+ \leq 2.25$), (b) transitional roughness surface ($2.25 < K_s^+ \leq 90$), and (c) fully rough surface ($K_s^+ > 90$). According to these regimes, roughness effects are insignificant in the hydrodynamically smooth surface, but become gradually serious in the transitional roughness surface, and take full effect in the fully rough surface. The viscous sublayer, which is the region near the wall where is dominantly influenced by the viscous force, is fully established in the hydrodynamically smooth surface. However, the viscous sublayer is gradually disturbed by increasing roughness in the transitional roughness surface, so the viscous effect becomes decreasingly important. Finally, the viscous sublayer cannot be remained as a result of intense disturbance caused by roughness, thereby ignoring the viscous effect in the fully rough surface. The K_s^+ value is associated with computing shear stress (τ_w) at walls through the adaptive constant (ΔB) as a correlation proposed by Cebeci and Bradshaw [28] in Eq. (2)

$$\Delta B = \begin{cases} 0 \Leftrightarrow K_s^+ \leq 2.25 \\ \dfrac{1}{\kappa}\ln\left(\dfrac{K_s^+ - 2.25}{87.75} + C_s K_s^+\right) \cdot \sin[0.4258(\ln(K_s^+) - 0.811)] \\ \qquad \Leftrightarrow 2.25 \;\; K_s^+ \leq 90 \\ \dfrac{1}{\kappa}\ln(1 + C_s K_s^+) \Leftrightarrow K_s^+ > 90 \end{cases} \tag{2}$$

Then, the shear stress at the wall and other wall functions for the mean temperature and turbulent quantities are computed by the formula in Eq. (3)

$$\frac{u_p u^*}{\tau_w/\rho} = \frac{1}{\kappa}\ln\left(E\frac{u^* y_p}{\nu}\right) - \Delta B \tag{3}$$

where u_p, y_p, E, and κ are the mean velocity of the fluid at the wall-adjacent cell centroid, the distance from the centroid of the wall-adjacent cell to the wall, the empirical constant (=9.793), and the von Karman constant (=0.4187), respectively. For the model of the applied sand-grain roughness, the roughness level affects $y+$ values, thus causing the shift of the wall and the $y+$. As a result, the automatic near-wall treatment is switched into the wall function mode according to requirements. For heat transfer impact, the increasing surface roughness typically leads to an increase in turbulence production near the wall. Consequently, this can result in significant increases not only in the wall shear stress but also in the wall heat transfer coefficients as the turbulent viscosity (μ_t) increases with the level of turbulence caused by the roughness. In this work, the roughness constant is set as 0.5 in accordance with the instruction of the uniform sand-grain roughness model. The roughness height which is considered as the parameter study is set as 5, 10, and 20 μm. At these studied roughness heights, it is expected that the transitional roughness regime becomes dominant.

For the setup of boundary conditions, basically, boundary conditions reported by Timko [29] are used. Namely, the hot mainstream enters the inlet cascade with a uniform total temperature of 709 K and a uniform total pressure of 3.4474×10^5 Pa. The pressure ratio (PR), which is the ratio of the total pressure at the mainstream inlet to the static pressure at the mainstream outlet, is set as 1.67. Air coolant is supplied through the two cavities with a counterflow-path pattern. The total temperature and the total pressure of the coolant at the two inlets of the cavities are uniformly set as 339 K and 3.5095×10^5 Pa, respectively. In addition, freestream turbulence intensity (Tu) of the mainstream is 10%, whereas turbulence length scales (Lu) at the inlets and the outlet are the same values as the previous study [25]. These values are estimated by the correlation: $Lu = 0.07D_h$, where D_h is the hydraulic diameter of the inlet and outlet. The boundary condition of the mainstream cascade is periodic with the rotational angle of 7.826 deg. All boundary conditions are summarized in Table 2, and Fig. 6 displays some parts of the boundary conditions used in this work. For the aerothermal property of the materials, the vane material, mainstream and coolant, and TBC are made of steel, air, and ZrO_2, respectively. Thermal conductivity and specific heat capacity of steel and air are expressed linearly in terms of temperature. Air is assumed to obey the ideal gas law and its viscosity is computed by Sutherland law. All properties of TBC are constant. Table 3 lists all material properties used in the present work.

Numerical Validation and Simulation Cases

As the geometry of the vane and the computational mesh are the same as Zhang et al. [25], the validation of numerical results obtained by SST k–ω model and approved by Zhang et al. [25] is used. It should be noted that this validation was conducted at $PR = 2.50$ and the numerical result in terms of the Mach number (Ma) distribution along the vane surface at 50% span was compared with the Ma distribution obtained by experiment reported by Timko [29], as shown in Fig. 7. Clearly, the SST k–ω model provides acceptable Ma in general, except in the region with the range of $0.65 < x/C < 0.75$ where lacks enough experimental data. However, it seems that such a region is likely to be under the influence of shock emanating from the neighbor vane, as previously studied by Xu et al. [30]. Another thing that should be mentioned here is that the thermal validation has not been verified yet due to a lack of experimental data of heat transfer from Timko [29] and other works. Inevitably, the present work needs to conduct the prediction of the cooling performance under the assumption that the aerodynamics of fluid flow is of fundamental importance to the heat transfer process accordance with the governing equations of fluid flow and heat transfer,

Table 2 Boundary conditions [23,25,29]

Boundary	Condition
Mainstream inlet	$T_\infty = 709$ K, $P_{T,\infty} = 3.4474 \times 10^5$ Pa, $Tu = 10\%$, $Lu = 0.4$ cm
Mainstream outlet	PR = 1.67, $Lu = 0.305$ cm
Forward coolant inlet	$T_c = 339$ K, $P_{T,c} = 3.5095 \times 10^5$ Pa, $Tu = 5\%$, $Lu = 0.064$ cm
Forward coolant outlet	Adiabatic wall with nonslip condition
Aft coolant inlet	$T_c = 339$ K, $P_{T,c} = 3.5095 \times 10^5$ Pa, $Tu = 5\%$, $Lu = 0.038$ cm
Aft coolant outlet	Adiabatic wall with nonslip condition

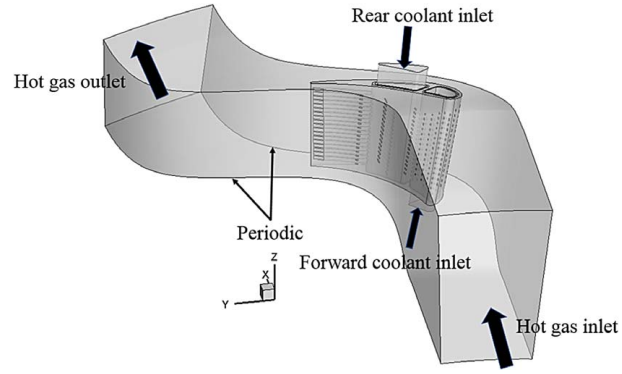

Fig. 6 Major parts of boundary condition

Table 3 Details of material properties [23,25]

Property	Steel	Air	ZrO_2
Density (kg/m^3)	8055	Ideal gas	5500
Thermal conductivity (W/(m·K))	11.2 + 0.0144T[a]	0.01019 + 0.000058T[a]	1.04
Specific heat capacity (J/(kg·K))	438.5 + 0.177T[a]	938 + 0.196T[a]	418
Viscosity (kg/(m·s))	–	Sutherland law	–

[a]T in Kelvin.

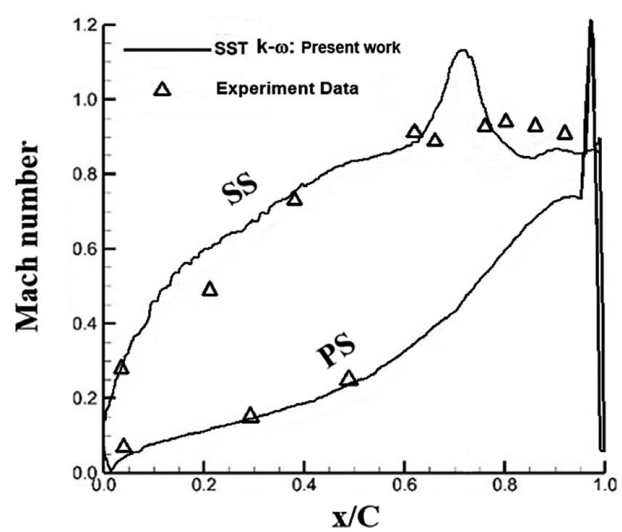

Fig. 7 Validation of Mach number obtained by SST k–ω model

Table 4 Simulation cases

Case	Condition
1	No surface roughness without TBC
2	$K_s = 5\ \mu$m without TBC
3	$K_s = 10\ \mu$m without TBC
4	$K_s = 20\ \mu$m without TBC
5	$K_s = 5\ \mu$m with TBC
6	$K_s = 10\ \mu$m with TBC
7	$K_s = 20\ \mu$m with TBC

including the equation of state for compressible flows. Therefore, the method which demonstrates the ability to a good acceptable aerodynamic agreement on the results of Mach number, pressure, and velocity distributions could provide a reasonable and acceptable thermal field, as seen in previously published literature [14,22,26,27,31,32]. Therefore, the validation of aerodynamic results done by Zhang et al. [25] is still meaningful for the thermal prediction and the solver with the SST k–ω model is used for the subsequent simulations.

To study the effects of surface roughness and combined effects of surface roughness and TBC on the cooling performances, seven cases of the simulation are conducted and listed in Table 4. Case 1 is calculated under the perfectly smooth vane without TBC. Cases 2–4 present results obtained from the uncoated vane under the effects of the increasing physical surface roughness. Cases 5–7 show results obtained from the coated vane under the integration of surface roughness and TBC effects. The numerical results obtained from case 1 are used as the benchmarks for comparisons of the other cases. In addition, the other cases are compared with one another also in order to perform the influences of TBC and surface roughness.

Results and Discussion

Numerical results are carried out in terms of heat transfer parameters, i.e., cooling effectiveness (denoted as ϕ), TBC effectiveness (denoted as τ), and heat transfer coefficient (denoted as h) under the separate and combined effects of the surface roughness and TBC. According to the conjugate heat transfer approach, the cooling effectiveness, which is the normalized temperature for a conducting wall, represents the role of energy transfer driven by the mechanism of heat conduction within the vane structure as well as heat convection in thermal boundary layers. The TBC effectiveness is used to indicate how TBC affects the vane material through conductive heat transfer within the TBC layer. The heat transfer coefficient is used in calculating the amount of heat convection between the hot mainstream and the vane surface. Figure 8 indicates variables and the method of evaluating the cooling effectiveness, TBC effectiveness, and heat transfer coefficient when the vane is uncoated and coated with TBC. The effectiveness is defined as Eq. (4), whereas the heat transfer coefficient is defined as Eq. (5)

$$\phi \text{ or } \tau = \frac{T_\infty - T_{ref}}{T_\infty - T_{c,in}} \quad \text{where } T_{ref} = \begin{cases} T & \text{for } \phi \text{ (without TBC)} \\ T_{\text{TBC}} & \text{for } \phi_{\text{TBC}} \text{ (with TBC)} \\ T' & \text{for } \tau \text{ (with TBC)} \end{cases} \tag{4}$$

$$h = \frac{q_{flux}}{T_\infty - T_{ref}} \quad \text{where } T_{ref} = \begin{cases} T & \text{for } h \text{ (without TBC)} \\ T' & \text{for } h_{\text{TBC}} \text{ (with TBC)} \end{cases} \tag{5}$$

The total temperature of the mainstream (T_∞) is used to compute the heat transfer coefficient. In the case of the uncoated vane, ϕ and h are calculated based on the static temperature of the external vane surface, namely, $T_{ref} = T$. Differently, when the vane is coated with TBC, T_{ref} is replaced with T_{TBC} to show the effectiveness of the vane substrate below the TBC layer, denoted as ϕ_{TBC}. Besides, τ and h_{TBC} are computed based on the TBC surface temperature, denoted as T'. According to the definitions of the thermal parameters, ϕ and τ are always positive because in reality T_∞ is always higher that T_{ref} and $T_{c,in}$. However, h can be both positive and negative, depending on the phenomenon. A positive h indicates that heat transfers from the fluid to the wall. Oppositely, h shows a negative value if heat transfers from the wall to the fluid. It should be noted that heat transfer coefficient is based on conducting wall surface temperature and freestream temperature, as reported by Zhao and Wang [33].

Effects on Cooling Effectiveness

This section presents the effects of roughness and the integration of roughness and TBC on the cooling effectiveness. Distributions of ϕ and ϕ_{TBC} at different dimensionless axial chord positions (x/C) at 50% span are presented, as seen in Fig. 9. It should be noted that at the stagnation point, x/C is 0; along the PS, x/C is negative; along the SS, x/C is positive. Generally, the predicted results indicate that ϕ obtained from cases 2–4 and ϕ_{TBC} obtained from cases 5–7 have similar trends to ϕ obtained from the smooth prediction, case 1. By taking only the effect of the roughness height, ϕ changes decreasingly as compared with case 1, especially at $K_s = 10\ \mu$m and 20 μm for cases 3 and 4, respectively. These are different from case 2 ($K_s = 5\ \mu$m) as it is found that case 2 provides insignificant differences in ϕ for all positions of x/C. This can be explained by the fact that at $K_s = 5\ \mu$m, the average K_s^+ equals 1.82. According to Eq. (2), it indicates that the surface is hydraulically smooth and the surface roughness barely disturbs the viscous sublayer. Therefore, the aerothermal condition changes unaffectedly, thereby resulting in the surface temperature very slightly. However, at $K_s = 10\ \mu$m and 20 μm (the average $K_s^+ = 3.12$, and 4.55, respectively), these values of K_s^+ show that the surface ends to be hydraulically smooth and begins to show the effects of the roughness, namely, starting the transitionally rough regime. The predicted

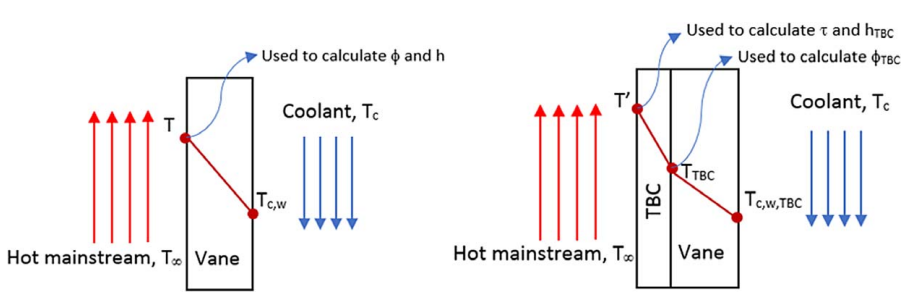

Fig. 8 Evaluation of heat transfer coefficient, cooling, and TBC effectiveness

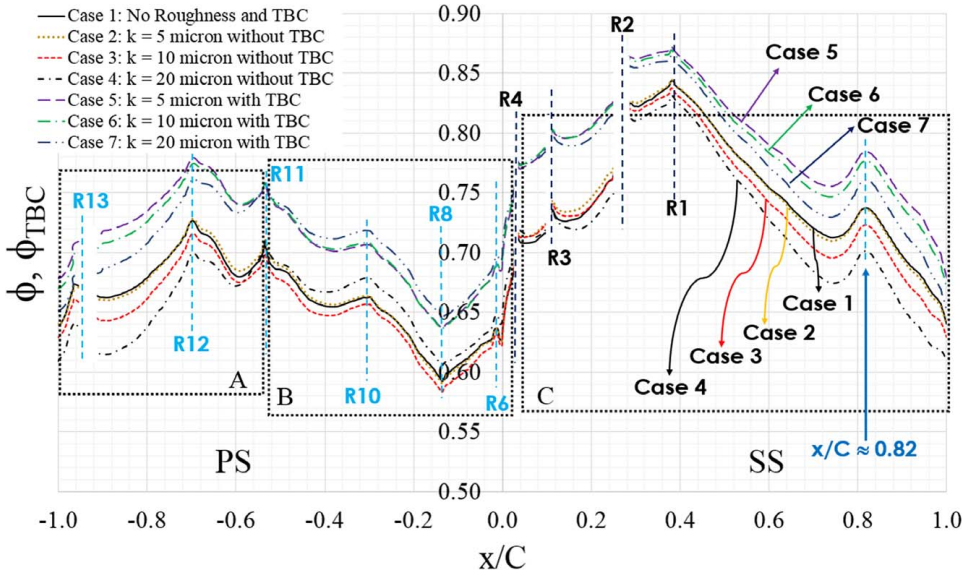

Fig. 9 ϕ and ϕ_{TBC} distributions at different roughness heights

results also point out the integration of roughness and TBC effects, that is, the values of ϕ_{TBC} predicted from cases 5–7 are much higher than those of ϕ obtained from case 1 and even cases 2–4 for all positions of x/C. This is unsurprising because a very low thermal conductivity of the TBC layer plays a major role as a good thermal insulator which affects unfavorably thermal conduction. Consequently, the values of T_{TBC} obtained from cases 5–7 are always lower than those of T obtained from cases 1–4. For further discussion, three interesting regions are found from the ϕ and ϕ_{TBC} distributions, i.e., (1) region A: the rear-half portion of the PS to the TE, $-1.0 < x/C < -0.55$; (2) region B: the suction-side vicinity of the LE to the further downstream on the PS, $-0.52 < x/C < 0.025$; and (3) region C: the SS to the TE, $0.04 < x/C < 1.0$. It is obvious that the roughness at $K_s = 5\ \mu$m takes the effect on ϕ and ϕ_{TBC} very slightly in the three regions, whereas ϕ and ϕ_{TBC} in the regions A and C decrease as K_s increases to 10 μm and 20 μm. This can be explained by the fact that the roughness takes the effect on the viscous sublayer of the local flow field near the walls increasingly when K_s increases. The increasing K_s leads to an increment in the level of local turbulence production and the turbulent viscosity (μ_t) near the walls, thereby increasing turbulent (k_t) and effective (k_{eff}) thermal conductivities. It, therefore, enhances an amount of heat transferring to the vane surface and leads to T and T_{TBC} rises in those regions. Nevertheless, this phenomenon is quite different from that observed in the region B. Namely, ϕ and ϕ_{TBC} decreases at $K_s = 10\ \mu$m but increases at $K_s = 20\ \mu$m. These phenomena probably happen because region B which is located in the SS-LE-PS region to the downstream on the PS has a lower level of turbulent kinetic energy (k) than the regions A and C. Besides, the region B is quite sensitive to mainstream and local turbulence quantities. When K_s increases, the viscous sublayer is disturbed more and more by the roughness since the effect of the roughness becomes important increasingly and local turbulence production increases. Moreover, there are a lot of film holes in this region. These lead to significant differences in complicated local flow fields near the vane surface, as visibly shown in Fig. 10, thereby causing the uncertain prediction of local heat transfer, and ϕ and ϕ_{TBC} with K_s in the region B.

Figure 9 also shows that the variations of ϕ_{TBC} under the increase in the roughness height are lower than those of ϕ. This is also because of the high thermal resistance obtained by a great influence of the very low thermal conductivity of the TBC material, causing the strong difference between T' and T_{TBC}, as presented in terms of τ and shown in Fig. 11. Apart from the previous discussions, ϕ and ϕ_{TBC} in the locations which are close to the exit of film holes need to be provided. Figures 9 and 11 also indicate that for all the roughness heights, relatively high ϕ, ϕ_{TBC}, and τ are contributed by film holes from all rows, except row 8 which provides relatively low values. The maximum ϕ_{TBC} and ϕ are 0.872 and 0.844, respectively, at $K_s = 5\ \mu$m at the exit of the film hole of the row R1. This discrepancy is explained by the heat transfer parameter in the section: Effects on Heat Transfer Coefficient. In addition, for all cases of simulation, ϕ, ϕ_{TBC}, and τ in the region C decrease in the streamwise direction, except in the region with a range of about $0.75 < x/C < 0.82$ where ϕ, ϕ_{TBC}, and τ rise with x/C and are relatively high at $x/C \approx 0.82$. A plausible explanation is due to the presence of transitional flow in such region and this leads to heat transfer enhancement which is confirmed by the distribution of heat transfer coefficient in the next section. Another reason may be because such region has a narrow shape and the aft cavity is connected to the 18-channel slot film holes of the row R13. Thus, internal cooling and heat conduction become more dominant, thereby resulting in marked drops in T and T_{TBC}. However, these are different from T' which is considered on the TBC surface with high heat impedance. As a result, it leads to $T' > T > T_{\mathrm{TBC}}$ and $\tau < \phi < \phi_{\mathrm{TBC}}$ in such region.

To perform the separate and combined effects of the roughness and TBC on the whole region of the vane surface, holistic contours of ϕ and ϕ_{TBC} distributions on the PS including TE and LE, and SS including TE are presented, as seen in Figs. 12(*a*) and 12(*b*),

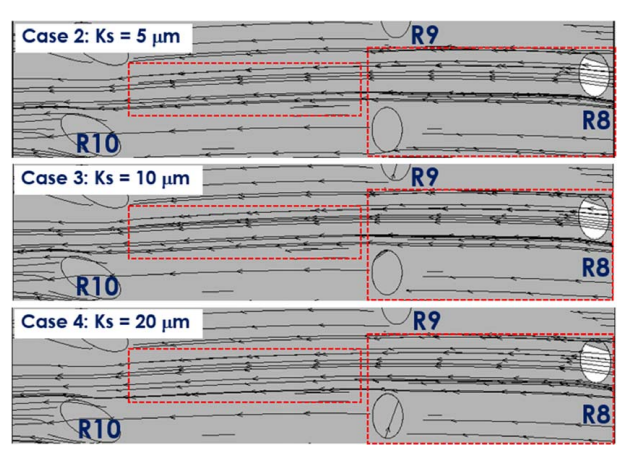

Fig. 10 Local flow field of mainstream in midspan region on PS at different roughness heights through 2500 streamlines

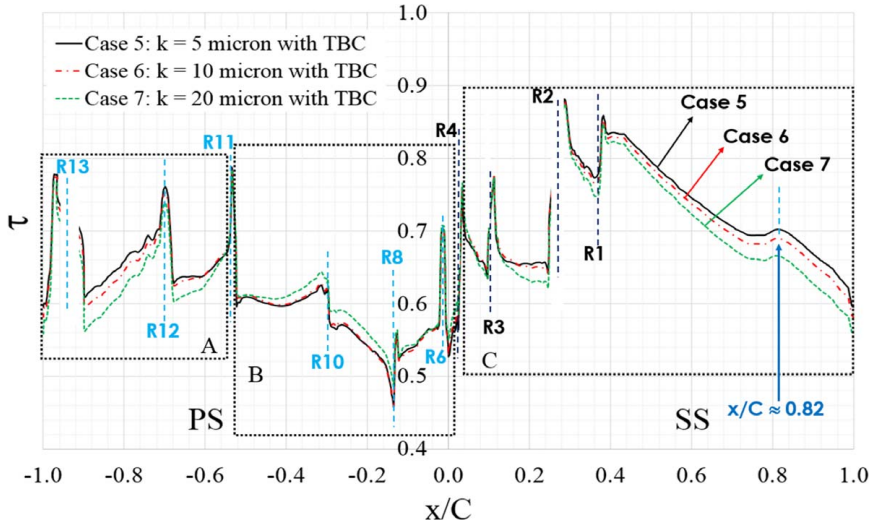

Fig. 11 τ **distributions at different roughness heights**

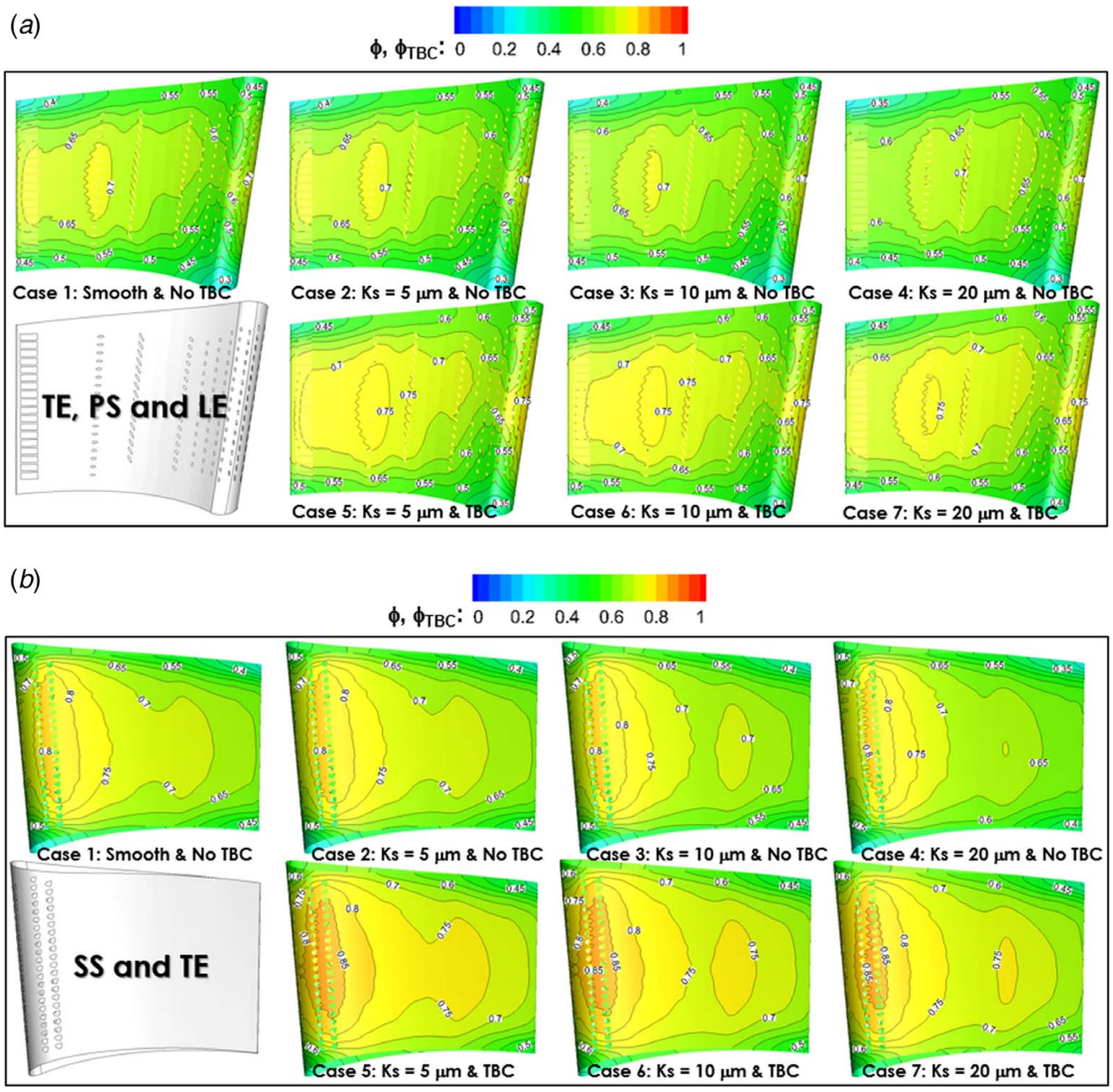

Fig. 12 ϕ **and** ϕ_{TBC} **distributions on (*a*) PS, LE, and TE and (*b*) SS and TE at different roughness heights**

respectively. These contours show that ϕ and ϕ_{TBC} distributions change as the roughness height increases. The contours also indicate that the distributions of ϕ and ϕ_{TBC} on the vane surface correspond to those obtained along the surface at midspan, as previously shown in Fig. 9, except in regions where are cooled ineffectively by the cooing air such as regions near the hub and the tip of the vane. Obviously, both ϕ and ϕ_{TBC} predicted from cases 1 to 7 in the regions near the hub and tip are markedly inferior to those in the regions where are close and near to the film holes. This is reasonable because the profound impact of film cooling provides relatively high ϕ and ϕ_{TBC} in such regions.

A better understanding of the effects of the roughness and TBC is discussed by comparing τ on the TBC surface and ϕ_{TBC} on the substrate vane on the PS including TE and LE, and SS including TE, as seen in Figs. 13(*a*) and 13(*b*), respectively. Evidently, the distributions of ϕ_{TBC} are much more uniform than those of τ for all the roughness heights, especially in the regions where are strongly influenced by cooling air from film holes such as the downstream of film holes. Of course, this suggests a major role of heat transfer within the vane structure driven by temperature gradients. However, it seems that when K_s increases, τ and ϕ_{TBC} alters similarly. The contours also indicate that in general for all roughness heights, τ is lower than ϕ_{TBC}, but τ may be higher than or equal to ϕ_{TBC} in regions where are close to the film holes.

To perform deeply the effects of the roughness and the combined effects of the roughness and TBC on ϕ and ϕ_{TBC}, PS and SS contours of the percentage difference of ϕ and ϕ_{TBC} are presented in Figs. 14(*a*) and 14(*b*), respectively. The percentage difference of ϕ and ϕ_{TBC} are denoted by $\Delta\phi$ and $\Delta\phi_{\mathrm{TBC}}$, and calculated as $\Delta\phi = \dfrac{\phi_{roughness} - \phi_{smooth}}{\phi_{smooth}}$ and $\Delta\phi_{\mathrm{TBC}} = \dfrac{\phi_{\mathrm{TBC},roughness} - \phi_{smooth}}{\phi_{smooth}}$, respectively. The contours indicate the significant difference between the

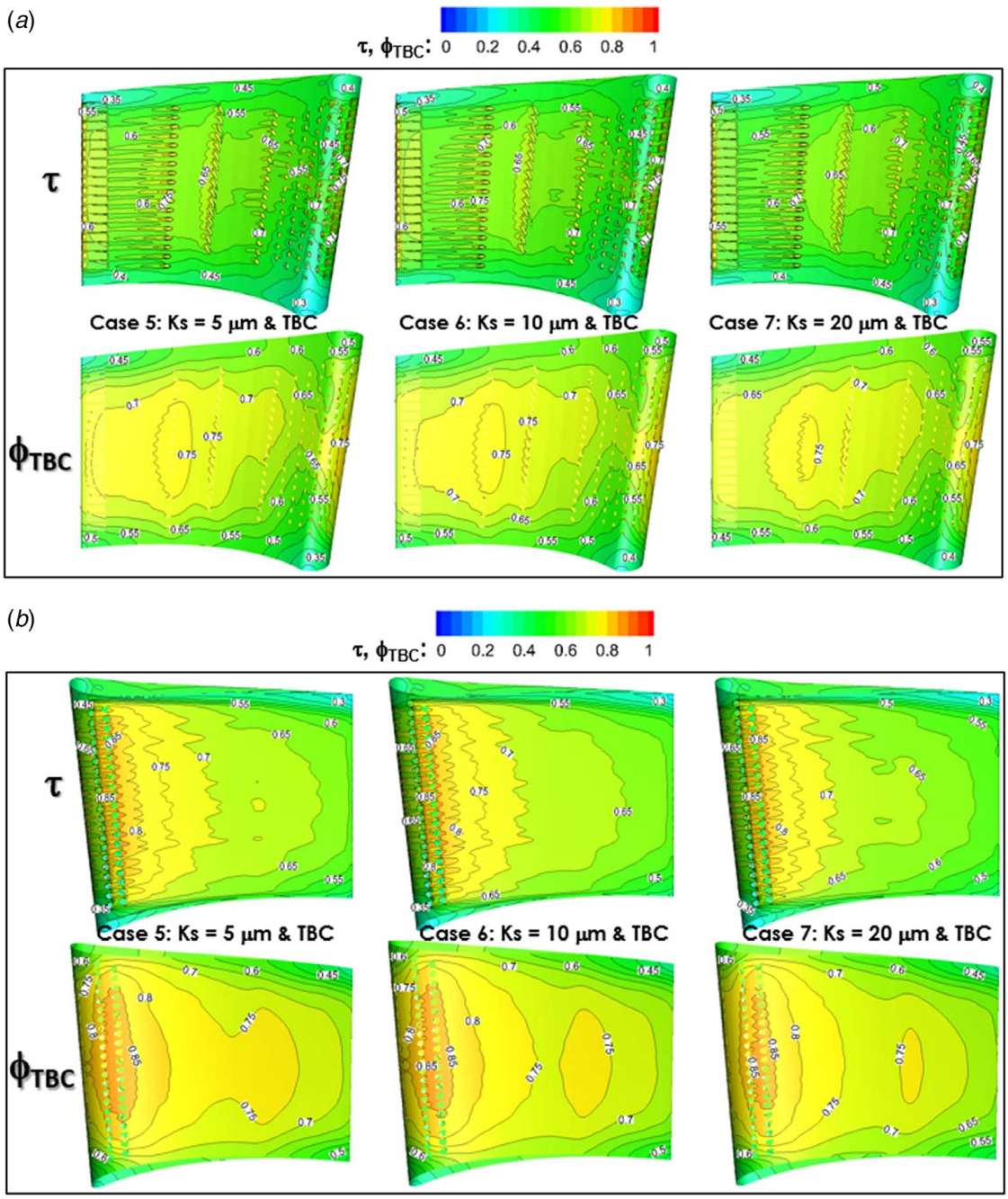

Fig. 13 τ **and** ϕ_{TBC} **distributions on (*a*) PS, LE, and TE and (*b*) SS and TE at different roughness heights**

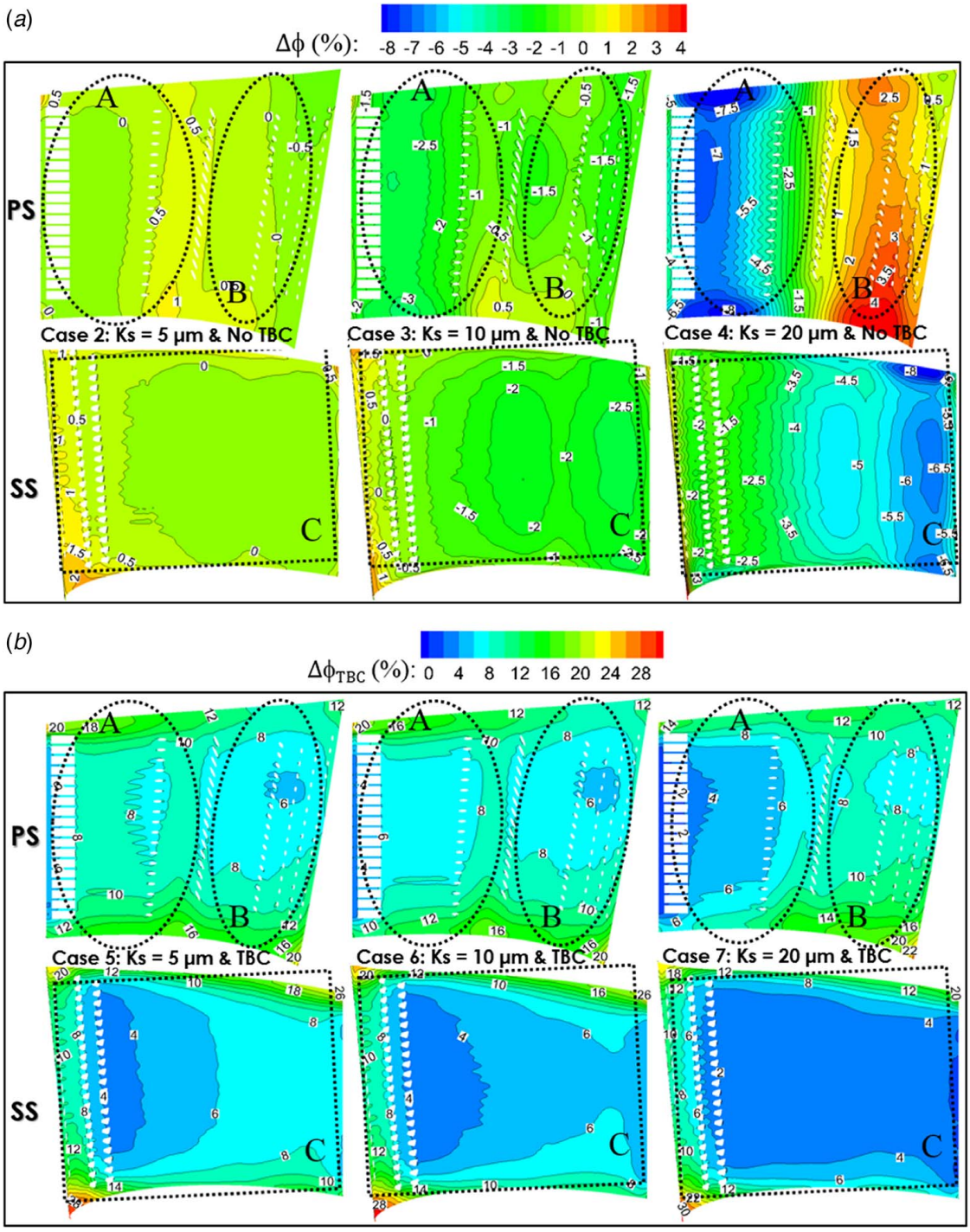

Fig. 14 $\Delta\phi$ **distributions on vane surface (*a*) without TBC and (*b*) with TBC at different roughness heights**

regions A, C, and B, where are consistent in Fig. 9. Undoubtedly, $\Delta\phi$ and $\Delta\phi_{\mathrm{TBC}}$ decrease with K_s in the regions A and C, but uncertainly vary with K_s in region B as explained previously. It can be seen that the $\Delta\phi$ and $\Delta\phi_{\mathrm{TBC}}$ in regions with the influence of film cooling are lower than those in the hub and the tip regions. Additionally, $\Delta\phi_{\mathrm{TBC}}$ is always positive and can reach as much as 30%. Nonetheless, $\Delta\phi$ can vary positively and negatively in the range of about −8% to 4%. These show the significance of the inclusion of TBC on the vane surface, which causes a great impact on the thermal protection directly. The presence of all the predicted phenomena of the cooling effectiveness is explained more by variations of the heat transfer coefficient in section Effects on Heat Transfer Coefficient.

Effects on Heat Transfer Coefficient

The effects of roughness and the combination of roughness and TBC on the heat transfer coefficient are discussed in this section. Distributions of h and h_{TBC} along the vane surface at midspan are presented, as seen in Figs. 15 and 16, respectively. Generally, both figures show a similar trend of the h and h_{TBC} distributions obtained from cases 1–7. With the influence of the roughness and TBC, it results in the heat transfer mechanism indirectly and directly. According to the three regions observed in the ϕ, ϕ_{TBC}, and τ distributions, these regions are also found correspondingly in the h and h_{TBC} distributions. In the regions A and C, it is

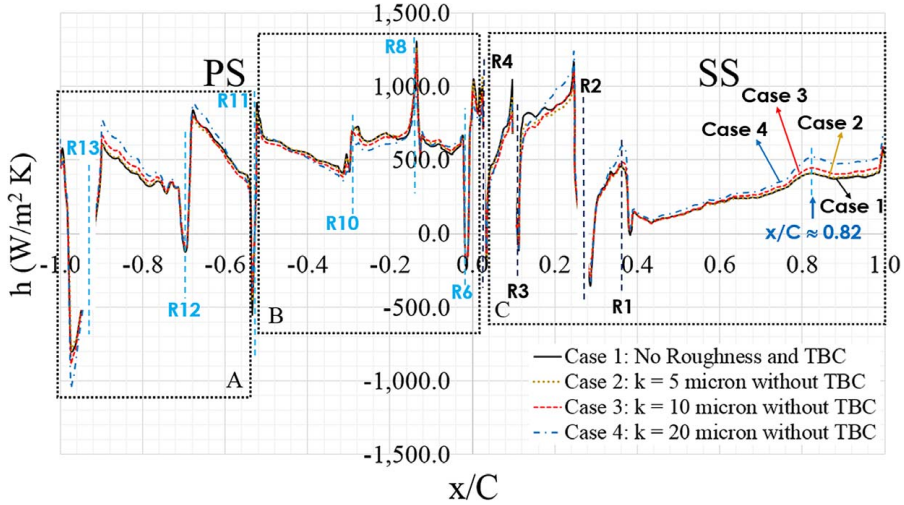

Fig. 15 Heat transfer coefficient distribution on vane surface without TBC

evident that h and h_{TBC} are augmented by increasing K_s, thereby declining in ϕ and ϕ_{TBC}, particularly at $K_s = 20\ \mu$m for both cases 4 and 7. Differently, the trends of the h and h_{TBC} variations in the region B are uncertain when K_s rises. These trends show consistent phenomena in the variations of ϕ and ϕ_{TBC}, which exist due to the thermal energy transfer in the complicated local flow fields near the surface as previously explained in section of the Effects on Cooling Effectiveness.

In addition, as mentioned that relatively high ϕ, ϕ_{TBC}, and even τ exist just in the downstream of the exit of the film holes, except the row R8. This may be clarified by heat transfer coefficients in Figs. 15 and 16 as well. The figures show that local heat transfer coefficients in the downstream regions of the exit of film holes with the relatively high ϕ, ϕ_{TBC}, and τ drop sharply, and h and h_{TBC} become negative. The reason is that as cooling air is injected into the hot mainstream, this reduces the temperature of the mixed fluid in these regions. The mixed fluid temperature is, therefore, lower than the surface temperature. As a result, heat transfers from the surface to the mixed fluid, thus causing low T, T_{TBC}, and T'. However, local heat transfer coefficients of the downstream of the exit of film holes from the row R8 surge drastically with positive values. This implies that the surfaces in the downstream of the exit of the film holes with the relatively high ϕ, ϕ_{TBC}, and τ are effectively cooled by the cooling air emitted from the film holes, as seen in Fig. 17 for an example of case 4. Contrarily, ineffective cooling air discharged by row 8 is attributed to the position and configuration of film holes which are in the radial direction on the PS. Moreover, it is possible that local pressures of the mainstream are higher than the pressure of the cooling air at the exit of the film holes of the row R8, thereby blocking the cooling air from the holes. This ineffectiveness results in relatively low ϕ, ϕ_{TBC}, and τ provided by the radial film holes at the midspan when compared with the other types of the film holes, for example, the row R11, as seen in Fig. 18 as well.

According to the improvement of ϕ and ϕ_{TBC} in the range of about $0.75 < x/C < 0.82$ in the region C as mentioned in the previous section, the investigation of the heat transfer coefficient indicates that flow becomes transitional in such region. Therefore, it leads to the improvement of the mixing stream between the hot mainstream and the cooling air. As a result, h and h_{TBC} increase and cause the increment in ϕ and ϕ_{TBC} in such region and the relatively high ϕ and ϕ_{TBC} at $x/C \approx 0.82$. However, at the same K_s, h_{TBC} is lower than h in general. This implies that the TBC layer, which has a very high thermal resistance, impedes the increasing heat transfer caused by the roughness increment. To further investigate the effects on the vane surfaces, Figs. 19(*a*) and 19(*b*) show PS and SS contours of the effect of the surface roughness and TBC on h and h_{TBC} in terms of Δh and Δh_{TBC} which are defined as

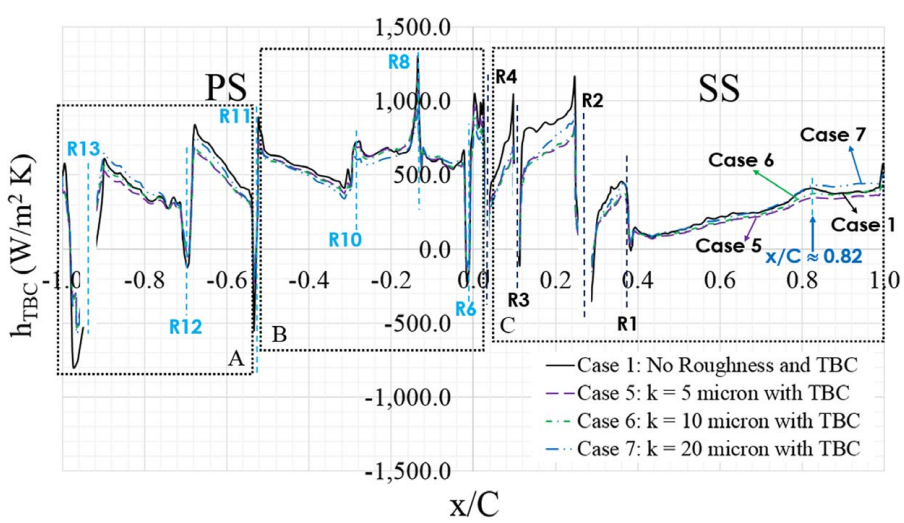

Fig. 16 Heat transfer coefficient distribution on vane surface with TBC

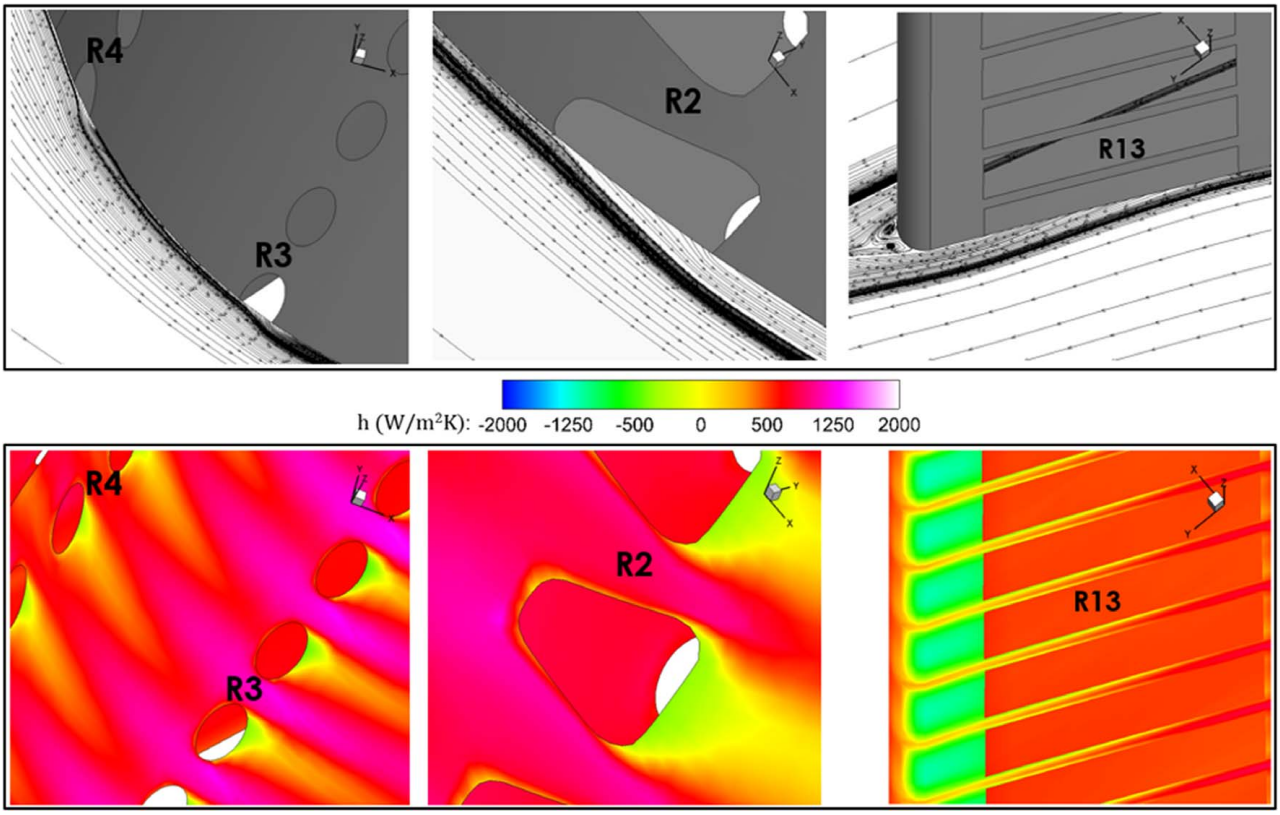

Fig. 17 Flow and heat transfer coefficient of cooling air on the downstream of film holes obtained from case 4

$\Delta h = h_{roughness} - h_{smooth}$ and $\Delta h_{\mathrm{TBC}} = h_{roughness,\mathrm{TBC}} - h_{smooth}$, respectively. Both figures also indicate the regions A, B, and C as mentioned previously. Visibly, variations of Δh and Δh_{TBC} on the PS and SS change in a similar way to the variations of $\Delta\phi$ and $\Delta\phi_{\mathrm{TBC}}$, respectively. With increasing in K_s, Δh, and Δh_{TBC} in the regions A and C become more positive, but become indeterminate in the region B. For all K_s values, Δh_{TBC} is much lower than Δh. These phenomena suggest the important role of the surface roughness for heat transfer enhancement and the inclusion of the TBC layer to mitigate increasing heat transfer caused by the growth of surface roughness. These can affect the cooling performances of the turbine vane.

Effects on Thermal Sensitivity

This section investigates vane thermal sensitivity to the separate and combined effects of the roughness and TBC. Average (Ave.), maximum (Max.), and minimum (Min.) cooling effectiveness which correspond to average, minimum, and maximum temperatures, respectively, are presented. It should be noted that the terms of "average, maximum, and minimum" are considered from the volume metal temperature and the cooling effectiveness is computed as Eq. (4), $\phi = \frac{T_\infty - T_{ref}}{T_\infty - T_{c,in}}$, where T_{ref} is the metal temperature of the vane based on the volume basis. Here, ϕ_{av}, ϕ_{max}, and ϕ_{min} represent the average, maximum, and minimum cooling effectiveness, respectively. The investigated range of the roughness is expanded to 120 μm to obtain a better understanding in the variation of the cooling performance under the roughness influence. Figure 20 shows that the improvement of ϕ_{av}, ϕ_{max}, and ϕ_{min} is attributed to the inclusion of TBC for all K_s values. The results also indicate that from $K_s = 20$–120 μm, ϕ_{av}, ϕ_{max}, and ϕ_{min} under the separate and combined effects of roughness and TBC decrease with the increment of K_s linearly. However, the declining trend of ϕ_{max} is slight. The reduction of ϕ_{av}, ϕ_{max}, and ϕ_{min} is related to the increment of the vane temperature, i.e., ΔT_{av}, ΔT_{min}, and ΔT_{max}, respectively, as seen in Fig. 21. In general, ΔT increases first, then decreases and finally seems stabilized when K_s increases. This phenomenon can be explained by the fact that (1) when $0 \le K_s < 5$ μm, the size of roughness elements is smaller than the viscous length scale. So, the roughness is too small to affect the flow, thereby insignificantly causing the heat transfer. As a result, ΔT depends upon the capability of TBC, so TBC plays an important and dominant role and ΔT is found large in this K_s range. (2) When $5 \le K_s < 60$ μm, this K_s range is in the transitional roughness surface. Therefore, the role of the surface roughness becomes important increasingly and its effect disturbs and competes with the viscous effects, thus enhancing heat transfer. Consequently, ΔT decreases significantly as K_s increases in this range. (3) When $K_s \ge 60$ μm, it seems that the roughness effects take over the viscous effect as a result of intense disturbance, thereby reducing the viscous effect drastically in this range. Therefore, ΔT decreases slower than the second regime and ΔT

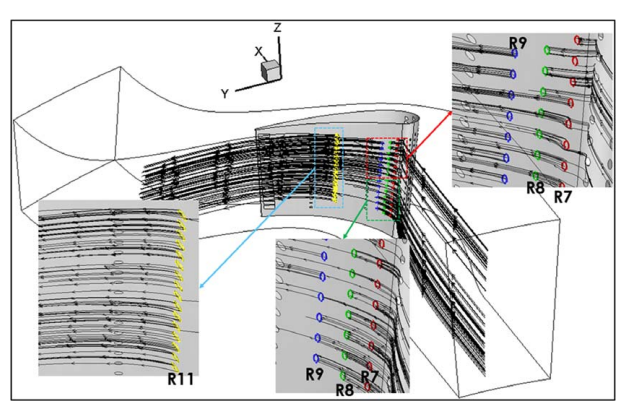

Fig. 18 Streamlines of cooling air emitted from film holes R7, R8, R9, and R11 for case 4

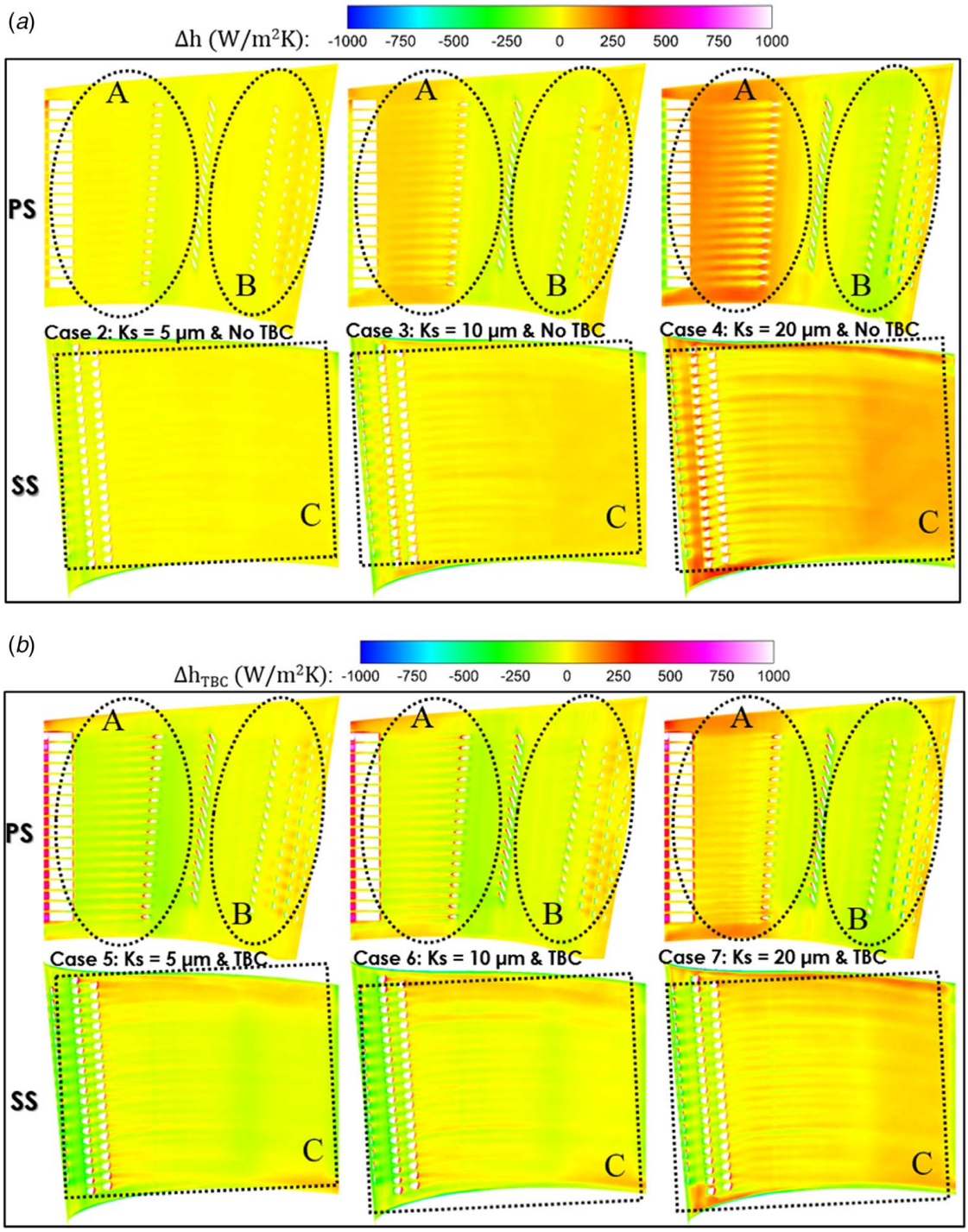

Fig. 19 Difference of heat transfer coefficient distribution on vane surface (*a*) without TBC and (*b*) with TBC

shows small differences as K_s increases. In addition, it is clear that without TBC, 24 K and 20 K rises of T_{ave} and T_{max}, respectively, are caused by the maximum roughness height, $K_s = 120\ \mu$m, but only 8.4 K increase in T_{min} is caused by this roughness height. These phenomena can be elucidated by the fact that normally T_{min} exists in the cold-wall side of the coolant passages, whereas T_{max} presents in the hot-wall side of the hot mainstream. With varying in K_s, the aerothermal condition on the vane surface of the hot-wall side is altered directly. This causes disturbances to the viscous sublayer increasingly and flow becomes turbulent increasingly. Consequently, the heat transfer from the hot mainstream to the vane surface is enhanced in accordance with $q_{flux} = -k_{eff}\partial\bar{T}/\partial y = -(k_l + k_t)\partial\bar{T}/\partial y$, where k_l is the laminar thermal conductivity and $\partial\bar{T}/\partial y$ is the wall temperature gradient. This can be noticeable through the increase in the effective thermal conductivity (defined by the sum of the laminar and turbulent thermal conductivities) of the mainstream at interfaces when K_s increases for with and without TBC, as seen in Fig. 22. As T_{max} increases significantly with the increasing K_s, this certainly causes the serious increment in T_{av} as well since the driving temperature from the hot-side and cold-side walls increases. Figure 21 also points out the favorable effects of TBC on T_{av}, T_{min}, and T_{max} of the rough vane. Namely, TBC reduces T_{av}, T_{max}, and T_{min} as much as 18 K, 27.8 K, and 8.6 K, respectively, at $K_s = 5\ \mu$m. Despite the

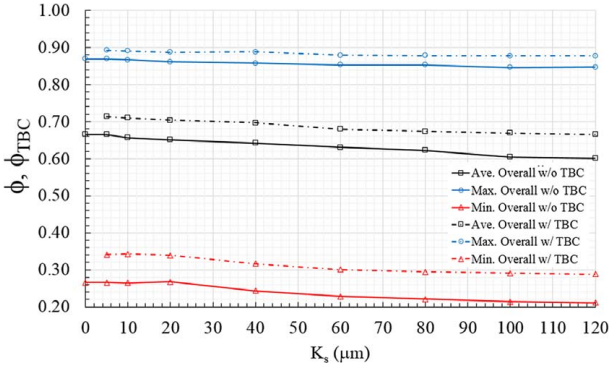

Fig. 20 Variations of ϕ_{av}, ϕ_{max}, and ϕ_{min} at different K_s values

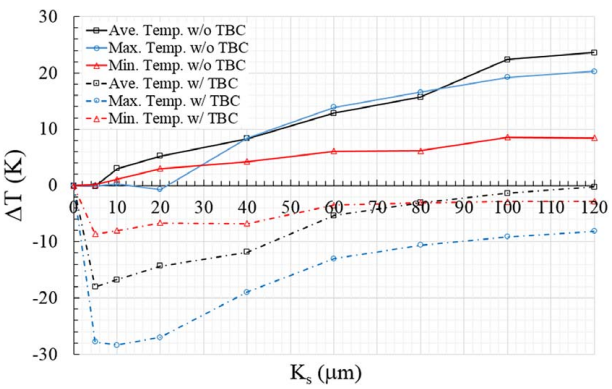

Fig. 21 Variations of ΔT_{av}, ΔT_{max}, and ΔT_{min} at different K_s values

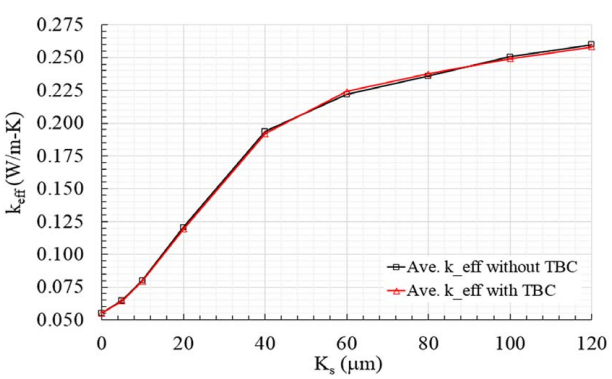

Fig. 22 Variations of average effective thermal conductivities of hot mainstream at interfaces

decline of the cooling performance with K_s, the presence of TBC alleviates the vane temperatures, as seen that ΔT_{av}, ΔT_{min}, and ΔT_{max} are still lower than 10 K at the maximum roughness height.

Conclusion

In this study, computational fluid dynamics with conjugate heat transfer analysis is applied to numerically investigate separate and combined effects of vane surface roughness and TBC on the cooling performance of a high-pressure turbine vane which is cooled by numerous film holes. Cooling effectiveness and heat transfer coefficient obtained by the prediction in an investigated range of the roughness height from 5 to 20 μm is presented and compared with that by the perfectly smooth vane. Results show that from the perfectly smooth vane to the rough vane with the maximum roughness height, in general, the roughness height increases local heat transfer coefficients in the rear-half portion of the pressure side to the trailing edge and the suction side to the trailing edge. This phenomenon leads to the deterioration of the cooling effectiveness in such regions. However, the local heat transfer coefficients change uncertainly with the surface roughness height in the suction-side vicinity of the leading edge to the further downstream of the pressure side, thereby causing the uncertainty in the cooling effectiveness in this region. Despite the fact that the increase in roughness height affects adversely the cooling performance, the cooling effectiveness is improved significantly due to heat transfer impedance from TBC. Without TBC, the cooling effectiveness varies within a range of −8% to 4%. However, due to TBC protection, the cooling effectiveness of the vane with TBC changes more widely with a range of 0–30%. To obtain a better understanding of the variation of the cooling performance under the roughness influence, the investigated roughness range is extended to 120 μm. Thermal sensitivity to the roughness height and TBC is investigated based on the volume basis. Results show that the surface roughness height has a significant effect on the cooling performance. Indeed, without TBC, a 120 μm increase in the roughness height results in 24 K and 20 K rises of the average and maximum vane temperatures, respectively. With the inclusion of TBC, the average and maximum vane temperatures are reduced as much as 18 K and 27.8 K, respectively. Despite the decline of the cooling performance with the roughness height, the presence of TBC alleviates the vane temperatures. The average and maximum vane temperatures are still lower than 10 K though roughness height reaches the maximum of 120 μm.

However, it should be mentioned that although the SST k–ω turbulence model, which is used for this work, can provide acceptable numerical results in terms of aerodynamics and heat transfer as reported in the open literature. The numerical prediction of this work obtained by the SST k–ω model is validated aerodynamically only, the heat transfer part is carried out under the favorable assumption of the governing equations of fluid flow and heat transfer, including the equation of state for compressible flows. Hence, the conclusion drawn here should be extended cautiously.

Acknowledgment

All support of the Institute of Mechanics, Chinese Academy of Sciences is gratefully acknowledged. The first author would like to express appreciation to the Chinese Academy of Sciences (CAS) for giving an opportunity to do research under the PIFI programme. In addition, the first author would like to express gratitude to Professor Jianhua Wang, Dr. Huazhao Xu, and Mr. Qingbo Zhang, University of Science and Technology of China for their support and guidance. Lastly, the first author is grateful for the full support of King Mongkut's Institute of Technology Ladkrabang.

Funding Data

- Chinese National Key Research and Development (R&D) Program (Grant No. 2017YFB1201304).
- National Natural Science Foundation of China (Grant No. 11702297; Funder ID: 10.13039/501100001809).
- Informatization Plan of the Chinese Academy of Sciences (Grant No. XXH13506-204).

Nomenclature

h = heat transfer coefficient
k = turbulent kinetic energy
E = empirical constant (=9.793)
T = temperature

U = velocity
h_{tbc} = heat transfer coefficient with TBC
k_{eff} = effective thermal conductivity
k_l = laminar thermal conductivity
k_t = turbulent thermal conductivity
q_{flux} = heat flux
u_p = mean velocity of fluid at wall-adjacent cell centroid
y_p = distance from centroid of wall-adjacent cell to wall
C_s = roughness constant
C_μ = constant (=0.09)
D_h = hydraulic diameter
K_s = physical roughness height
T_{av} = average temperature
T_c = coolant temperature
$T_{c,in}$ = temperature at coolant inlet
$T_{c,w}$ = temperature at cold-wall side without TBC
$T_{c,w,\mathrm{TBC}}$ = temperature at cold-wall side with TBC
T_{max} = maximum temperature
T_{metal} = metal temperature
T_{min} = minimum temperature
T_{ref} = reference temperature
T_{TBC} = substrate temperature
T_w = static wall temperature
T_∞ = total temperature at mainstream inlet
u^* = velocity parameter
T' = TBC temperature
K_s^+ = nondimensional roughness height
Lu = turbulence length scales
Ma = Mach number
PR = pressure ratio
Tu = turbulence intensity
ΔB = aptive constant
Δh = difference of heat transfer coefficient
ΔT_{av} = difference of average temperature
ΔT_{max} = difference of maximum temperature
ΔT_{min} = difference of minimum temperature
$\frac{\partial \bar{T}}{\partial y}$ = wall temperature gradient

Greek Symbols

$\Delta\phi$ = percentage difference of cooling effectiveness
$\Delta\phi_{\mathrm{TBC}}$ = percentage difference of cooling effectiveness with TBC
ν = kinematic viscosity
κ = von Karman constant (=0.4187)
ρ = density
ϕ = cooling effectiveness
ϕ_{av} = average cooling effectiveness
ϕ_{max} = maximum cooling effectiveness
ϕ_{min} = minimum cooling effectiveness
ϕ_{TBC} = cooling effectiveness with TBC
τ = TBC effectiveness
τ_w = wall shear stress

References

[1] Boynton, J. L., Tabibzadeh, R., and Hudson, S. T., 1993, "Investigation of Rotor Blade Roughness Effects on Turbine Performance," ASME J. Turbomach., **115**(3), pp. 614–620.
[2] Bunker, R. S., 1997, "Separate and Combined Effects of Surface Roughness and Turbulence Intensity on Vane Heat Transfer," ASME Paper No. 97-GT-135.
[3] Zhang, Q., Goodro, M., Ligrani, P. M., Trindade, R., and Sreekanth, S., 2005, "Influence of Surface Roughness on the Aerodynamic Losses of a Turbine Vane," ASME J. Fluid Eng., **128**(3), pp. 568–578.
[4] Bons, J. P., Taylor, R. P., McClain, S. T., and Rivir, R. B., 2001, "The Many Faces of Turbine Surface Roughness," ASME J. Turbomach., **123**(4), pp. 739–748.
[5] Bunker, R. S., 1997, "Effect of Discrete Surface Disturbances on Vane External Heat Transfer," ASME Paper No. 97-GT-134.
[6] Stripf, M., Schulz, A., and Wittig, S., 2005, "Surface Roughness Effects on External Heat Transfer of a HP Turbine Vane," ASME J. Turbomach., **127**(1), pp. 200–208.
[7] Matsuda, H., Otomo, F., Kawagishi, H., Inomata, A., Niizeki, Y., and Sasaki, T., 2006, "Influence of Surface Roughness on Turbine Nozzle Profile Loss and Secondary Loss," ASME Paper No. GT2006-90828.
[8] Neuhaus, L., Gilge, P., Seume, J. R., and Mulleners, K., 2016, "Influence of Surface Roughness on the Turbulent Properties in the Wake of a Turbine Blade," Proceedings of the 18th International Symposium on the Applications of Laser and Imaging Techniques to Fluid Mechanics, Lisbon, Portugal, July 4–7, pp. 1–21.
[9] Rutledge, J. L., Robertson, D., and Bogard, D. G., 2005, "Degradation of Film Cooling Performance on a Turbine Vane Suction Side due to Surface Roughness," ASME J. Turbomach., **128**(3), pp. 547–554.
[10] Demling, P., and Bogard, D. G., 2006, "The Effects of Obstructions on Film Cooling Effectiveness on the Suction Side of a Gas Turbine Vane," ASME Paper No. GT2006-90577.
[11] Nikuradse, J., 1933, "Laws for Flows in Rough Pipes," VDI-Forchungsheft Series B, 4 (English translation NACA TM 1292, 1950).
[12] Glasenapp, T., Puetz, F., Schulz, A., and Bauer, H. J., 2017, "Assessment of Real Turbine Blade Roughness Parameters for the Design of a Film Cooling Test Rig," ASME Paper No. GT2017-63088.
[13] Boyle, R. J., Spuckler, C. M., and Lucci, B. L., 2000, "Comparison of Predicted and Measured Turbine Vane Rough Surface Heat Transfer," ASME Paper No. 2000-GT-0217.
[14] Lutum, E., Cottier, F., Crawford, M. E., Laveau, B., and Abhar, R. S., 2015, "A Computational Investigation of the Effect of Surface Roughness on Heat Transfer on the Stator Endwall of an Axial Turbine," Proc. Inst. Mech. Eng., Part A, **229**(5), pp. 454–464.
[15] Boyle, R. J., 1994, "Prediction of Surface Roughness and Incidence Effects on Turbine Performance," ASME J. Turbomach., **116**(4), pp. 745–751.
[16] Roberts, S. K., and Yaras, M. I., 2004, "Boundary Layer Transition in Separation Bubbles Over Rough Surfaces," ASME Paper No. GT2004-53667.
[17] Stripf, M., Schulz, A., and Bauer, H. J., 2008, "Modeling of Rough Wall Boundary Layer Transition and Heat Transfer on Turbine Airfoils," ASME J. Turbomach., **130**(2), p. 021003.
[18] Bons, J. P., 2010, "A Review of Surface Roughness Effects in Gas Turbines," ASME J. Turbomach., **132**(2), p. 021004.
[19] Boyle, R. J., Parikh, A. H., Nagpal, V. K., Halbig, M. C., and DiCarlo, J. A., 2014, "Ceramic Matrix Composites for High Pressure Turbine Vanes," ASME Paper No. GT2014-27136.
[20] Feist, J. P., Sollazzo, P. Y., Berthier, S., Charnley, B., and Wells, J., 2012, "Application of an Industrial Sensor Coating System on a Rolls-Royce Jet Engine for Temperature Detection," ASME J. Eng. Gas Turbines Power, **135**(1), p. 012101.
[21] Sadowski, T., and Golewski, P., 2012, "The Analysis of Heat Transfer and Thermal Stresses in Thermal Barrier Coatings Under Exploitation," Defect Diffus. Forum, **326–328**, pp. 530–535.
[22] Alizadeh, M., Izadi, A., and Fathi, A., 2013, "Sensitivity Analysis on Turbine Blade Temperature Distribution Using Conjugate Heat Transfer Simulation," ASME J. Turbomach., **136**(1), p. 011001.
[23] Prapamonthon, P., Xu, H. Z., Yang, W. S., and Wang, J. H., 2017, "Numerical Study of the Effects of Thermal Barrier Coating and Turbulence Intensity on Cooling Performances of a Nozzle Guide Vane," Energies, **10**(3), p. 362.
[24] Halila, E. E., Lenahan, D. T., and Thomas, T. T., 1982, "Energy Efficient Engine High Pressure Turbine Test Hardware Detailed Design Report," NASA CR-167955, NASA Lewis Research Center.
[25] Zhang, Q., Xu, H., Wang, J., Li, G., Wang, L., Wu, X., and Ma, S., 2015, "Evaluation of CFD Predictions Using Different Turbulence Models on a Film Cooled Guide Vane Under Experimental Conditions," ASME Paper No. GT2015-42563.
[26] Ke, Z. Q., and Wang, J. H., 2016, "Conjugate Heat Transfer Simulations of Pulsed Film Cooling on an Entire Turbine Vane," Appl. Therm. Eng., **109(Part A)**, pp. 600–609.
[27] Yoshiara, T., Sasaki, D., and Nakahashi, K., 2011, Conjugate Heat Transfer Simulation of Cooled Turbine Blades Using Unstructured-Mesh CFD Solver. AIAA Paper No. 2011-457 498.
[28] Cebeci, C., and Bradshaw, P., 1977, *Momentum Transfer in Boundary Layers*, Hemisphere Publishing Corporation, New York.
[29] Timko, L. P., 1984, "Energy Efficient Engine High Pressure Turbine Component Test Performance Report," NASA CR-168289, NASA Lewis Research Center, Cleveland, OH.
[30] Xu, H. Z., Wang, J. H., and Wang, T., 2013, "Numerical Investigations of Wake and Shock Wave Effects on Film Cooling Performance in a Transonic Turbine Stage: Part 1-Methodology Development and Qualification Over Stationary Stators and Rotors," ASME Paper No. GT2013-94544.
[31] Mangani, L., Cerutti, M., Maritano, M., and Spel, M., 2010, "Conjugate Heat Transfer Analysis of NASA C3X Film Cooled Vane With an Object-Oriented CFD Code," ASME Paper No. GT2010-23458.
[32] Liu, J. H., Liu, Y. B., He, X., and Liu, L., 2016, "Study on TBCs Insulation Characteristics of a Turbine Blade Under Serving Conditions," Case Study Therm. Eng., **8**, pp. 250–259.
[33] Zhao, L., and Wang, T., 2012, "An Investigation of Treating Adiabatic Wall Temperature as the Driving Temperature in Film Cooling Studies," ASME J. Turbomach., **134**(6), p. 061032.